IEEE Photonics Journal
An IEEE Photonics Society Publication

Open Access

Compact Bidirectional Polarization Splitting Antenna

Volume 4, Number 5, October 2012

Fan Lu
Guangyuan Li, Member, IEEE
Feng Xiao, Member, IEEE
Anshi Xu, Member, IEEE

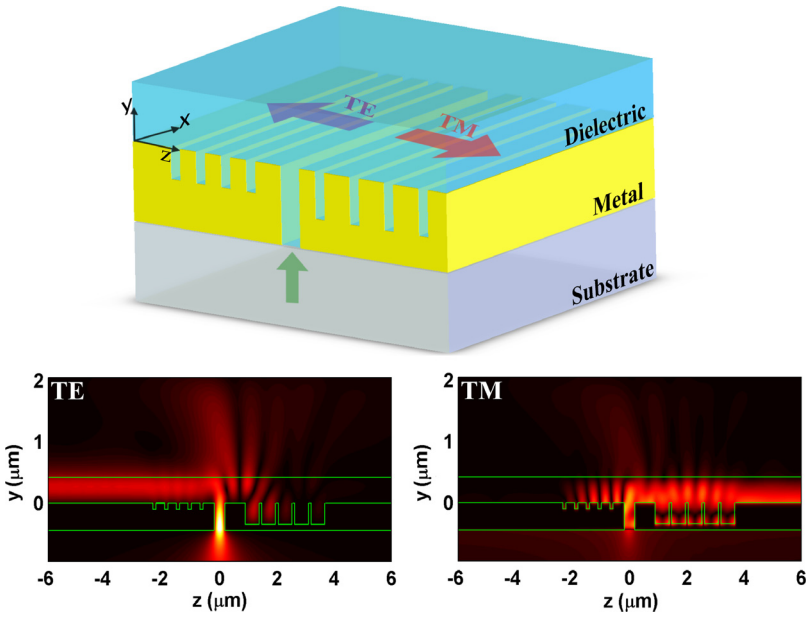

DOI: 10.1109/JPHOT.2012.2215020
1943-0655/$31.00 ©2012 IEEE

Compact Bidirectional Polarization Splitting Antenna

Fan Lu,[1] Guangyuan Li,[1] *Member, IEEE*, Feng Xiao,[2] *Member, IEEE*, and Anshi Xu,[1] *Member, IEEE*

[1]State Key Laboratory of Advanced Optical Communication Systems and Networks, School of Electronics Engineering and Computer Science, Peking University, Beijing 100871, China
[2]WA Center of Excellence for MicroPhotonic System, Electron Science Research Institute, Edith Cowan University, Joondalup, WA 6027, Australia

DOI: 10.1109/JPHOT.2012.2215020
1943-0655/$31.00 ©2012 IEEE

Manuscript received July 3, 2012; revised August 11, 2012; accepted August 20, 2012. Date of publication August 23, 2012; date of current version September 6, 2012. This work was supported in part by the National Natural Science Foundation of China (NSFC) under Grant 61107065 and in part by the China Postdoctoral Science Foundation. Corresponding author: G. Li (e-mail: gyli_2008@hotmail.com).

Abstract: A compact bidirectional polarization splitting antenna (BPSA) composed of a patterned metallic structure coated by a thin dielectric film is proposed and theoretically investigated. Using a polarization-selective array of grooves, the backside illuminated light transmitted through the central nanoslit is split and coupled into TM- and TE-polarized modes supported by the metal–dielectric–air (MDA) configuration. The operation principle of the structure is clarified and theoretically illustrated by utilizing the fully vectorial aperiodic Fourier modal method (a-FMM). Numerical simulations show that insertion losses (ILs) less than 4 dB, polarization extinction ratios (PERs) better than 18 dB, and crosstalk (CR) less than −18 dB are achieved for both polarizations in the wavelength range 1510–1570 nm. The structure will find potential applications in highly integrated polarization diversity systems and photonic integrated circuit.

Index Terms: Engineered photonic nanostructures, micro and nano antennas, subwavelength structures.

1. Introduction

Polarization-transparent microphotonic devices, spectral imaging and sensing techniques, and polarization diversity schemes in optical communication rely on structures that collect and sort photons by polarization [1]–[3]. The strong push for chip-scale integration has initiated a demand for very small subwavelength optical components and fomented great interest in identifying the ultracompact possible structures. Surface plasmon polaritons (SPPs) have made a breakthrough in the domain of photonic integration and interconnection by opening the possibility of overcoming the diffraction limit encountered in classical optics [4], [5]. The optical coupling from freely propagating light to SPPs has enabled many important functionalities, including the efficient unidirectional nanoslit coupler [6], plasmonic light beaming [7], bidirectional plasmonic splitter [8], compact antenna [9], and submicron plasmonic dichroic splitter [10].

Recently, the metal–dielectric–air (MDA) configuration consisting of a metal surface coated by a thin dielectric film has attracted much attention as a popular plasmonic waveguide, which has great potential for directional beaming of light [11], bidirectional wave coupler [12], rainbow trapping [13], and future plasmonic circuitry [14]–[16]. It is well known that both polarizations are important for many applications, such as integrated polarization diversity systems in optical communication [2],

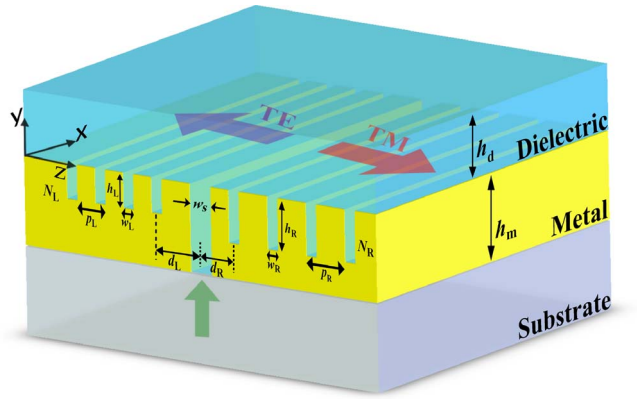

Fig. 1. Schematic of the proposed BPSA. The structure is composed of a nanoslit of width w_s surrounded by asymmetric periodic grooves of width, height, period, and number denoted by w_L, h_L, p_L, N_L and w_R, h_R, p_R, N_R on the left and right sides, respectively. The slit–groove distances on the left and right sides are d_L and d_R, respectively.

[17], [18]. However, most plasmonic applications are based on TM polarization only. As a matter of fact, the TE polarization analogous phenomena such as enhanced optical transmission [19], [20], beaming and focusing [21], and slit coupling [22] are attractive and have been demonstrated experimentally or theoretically. Fortunately, it has been shown that both TE- and TM-polarized modes could be supported by the MDA waveguide if the thickness of the dielectric film is properly chosen [23]. Thus, both polarizations could be exploited in the MDA waveguide, opening up a range of opportunities for new potential applications in photonic integration.

In this paper, we propose and theoretically analyze a compact bidirectional polarization splitting antenna (BPSA) based on a patterned metallic structure coated by a thin dielectric film. We show that the periodic array of grooves imposed on the MDA configuration has the feature of polarization selectivity: high reflection for one polarization and, meanwhile, high transmission for the other. Utilizing this property, we then design a BPSA composed of asymmetric grooves surrounding a nanoslit, which enables the backside illuminated light to be split and coupled into TM- and TE-polarized modes. Its operation principle will be clarified, and the performance will be investigated and discussed.

2. Structure and Operation Principle

Fig. 1 shows the proposed BPSA: It is composed of a slit of width w_s and surrounding asymmetric grooves milled in an optically thick metal film of thickness h_m deposited on a glass substrate $(n_s = 1.46)$. A thin dielectric film of thickness h_d is then added on top of the slit and grooves, which could provide additional benefit as a protection layer for metal to avoid oxidation in reality. The structure is under backside illumination of a normally incident unpolarized beam, and both TM- and TE-polarized modes supported by the MDA waveguide will be excited. We should note that backside illumination used here is favorable as it eliminates the possible significant noise introduced by the incident light, which then leads to a decrease in the system size [24], [25]. In this paper, silver with frequency-dependent permittivities tabulated in [26] is used as the metal film, and the refractive index of the dielectric film is assumed to be $n_d = 2.0$. Without special specifications, the operation wavelength is set to be $\lambda = 1550$ nm.

Fig. 2 presents the variation of the effective refractive index n_{eff} with thickness h_d of the dielectric film for different TE- and TM-polarized modes. The fundamental TM mode is the plasmonic mode bound to the metal surface with field decaying exponentially in the y-direction, while the TE mode is the photonic mode confined mainly in the dielectric film with relatively low propagation loss. For very thin dielectric film, the fundamental TM mode becomes progressively close to an SPP propagating along the metal–air interface [23]. The dependence of n_{eff} on h_d gives details that are needed to tune the effective refractive index for both polarized modes in the MDA waveguide. Both TE- and

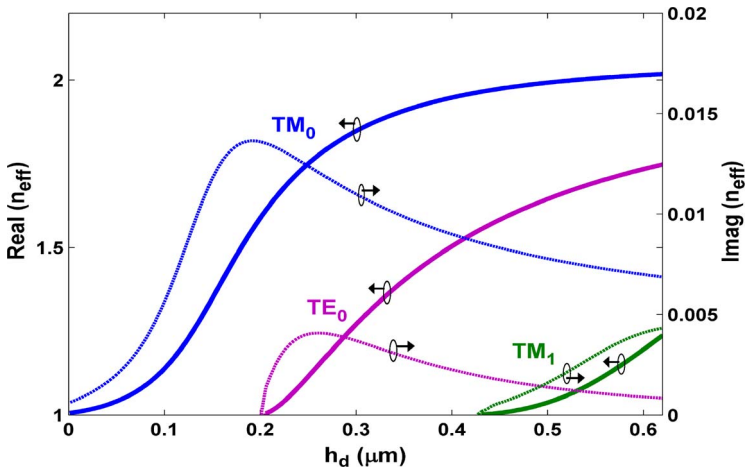

Fig. 2. Calculated dependence of the real and imaginary parts of the effective refractive index n_{eff} of TE- and TM-polarized modes supported by the MDA waveguide on the dielectric film thickness h_d.

TM-polarized modes could be supported by the MDA waveguide if the dielectric thickness is properly chosen. The thickness h_d is set to be 400 nm here so that both fundamental TE- and TM-polarized modes are of relatively low propagation loss.

We first show that a groove array may exhibit strong polarization selectivity in terms of reflectance and transmittance. The polarization-dependent reflection may be obtained when the period of the groove array satisfies the Bragg reflection condition expressed as [6], [27]

$$k_0 \mathrm{Re}\left(n_{\text{eff}}^{\text{TE;TM}}\right) p \approx m\pi \tag{1}$$

where $k_0 = 2\pi/\lambda$ is the wave vector in the vacuum, $n_{\text{eff}}^{\text{TE;TM}}$ is the effective refractive index of the fundamental TE- or TM-polarized mode, p is the period of the array, and m is an integer. As n_{eff} is polarization dependent, it is possible to realize high reflection of one polarization and simultaneously high transmission of the other for the same array of grooves. The reflectance and transmittance depend on the groove geometry (width and depth) and the number of grooves, and could be calculated efficiently following the theoretical models we have set up and validated in [28] and [29]. According to (1), the periods of asymmetric groove arrays are set to be $p_L = 410$ nm to reflect TM-polarized mode and $p_R = 570$ nm to reflect TE mode, respectively.

Throughout this paper, an analysis will be performed with $h_d = 400$ nm, $h_m = 450$ nm, and $w_s = 360$ nm. The numbers of grooves on both sides are set to be $N_L = N_R = 5$, which is adequate to offer a good performance of polarization splitting and also helps to minimize the device size. Specifically, for the left-side grooves of the proposed structure, the TM-polarized mode is efficiently reflected while the TE-polarized mode efficiently transmits; for the right-side ones, the performance of TM- and TE-polarized modes reverses. Our intuitive explanation of the polarization splitting operation has been made quantitatively by examining the grooves' scattering data using the fully vectorial aperiodic Fourier modal method (a-FMM) [30]. Fig. 3 shows the transmittance and reflectance as a function of the groove size. For some special groove sizes (indicated by the white "$\times$" signs in Fig. 3), the transmittance is high for one polarization, and meanwhile, the reflectance is also high for the other. As a result, it is suitable to set $w_L = 110$ nm and $h_L = 100$ nm for the left-side groove array and $w_R = 505$ nm and $h_R = 350$ nm for the right-side groove array. We notice that wider and deeper grooves are needed to obtain high reflectance of the TE-polarized mode. This is because the propagating TE mode is confined mainly in the dielectric film and, thus, is less sensitive to the roughness of the metal–dielectric interface. Moreover, the outward-going radiation scattered by grooves is small as $T + R$ for both polarizations are high.

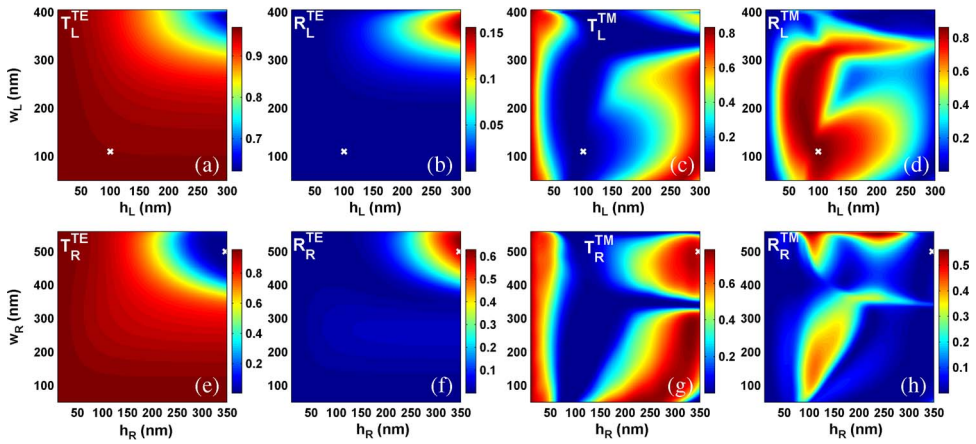

Fig. 3. Transmittance (T) and reflectance (R) of asymmetric groove arrays with $p_L = 410$ nm, $N_L = 5$ (a)–(d) and with $p_R = 570$ nm, $N_R = 5$ (e)–(h) at $\lambda = 1550$ nm as functions of groove width and depth. The white markers "×" denote the groove sizes for high TE transmittance and meanwhile high TM reflectance (top panel) or high TM transmittance and meanwhile high TE reflectance (bottom panel).

The slit–groove distances are also important for the performance of the BPSA. The TM-polarized mode reflected by the left grooves should interfere constructively with the one leaving the slit to the right, and the TE-polarized mode reflected by the right grooves should interfere constructively with the one leaving the slit to the left. This can be realized if

$$\arg\left(\rho_{N_L}^{\mathrm{TM}}\right) + 2k_0 \mathrm{Re}\left(n_{\mathrm{eff}}^{\mathrm{TM}}\right) d_L + \arg(\tau^{\mathrm{TM}}) = 2m_1\pi \tag{2a}$$

$$\arg\left(\rho_{N_R}^{\mathrm{TE}}\right) + 2k_0 \mathrm{Re}\left(n_{\mathrm{eff}}^{\mathrm{TE}}\right) d_R + \arg(\tau^{\mathrm{TE}}) = 2m_2\pi \tag{2b}$$

where m_1 and m_2 are integers; $\rho_{N_L}^{\mathrm{TM}}$ and $\rho_{N_R}^{\mathrm{TE}}$ are the reflectance coefficients of the left and right groove arrays, respectively; and τ^{TM} and τ^{TE} are the transmittance coefficients of the TM- and TE-polarized modes at the slit, respectively. As a result, the TE-polarized mode unidirectionally propagates to the left while the TM-polarized one to the right, resulting in an effective BPSA. Note that the phases introduced by the polarization-selective grooves' reflection have been embodied by the first terms of (2).

To check the validity of (2), we calculate a parameter I_r^{TM} (or I_r^{TE}) defined as the quotient between the squared of the field amplitude $|H_x|$ (or $|E_x|$) of the right-propagating TM mode (or the left-propagating TE mode) with grooves on both sides and without any grooves. Specifically, $I_r^{\mathrm{TM}} = |H_x^g|^2/|H_x^{wg}|^2$ and $I_r^{\mathrm{TE}} = |E_x^g|^2/|E_x^{wg}|^2$, where $|H_x^g|$ and $|E_x^g|$ are the maximum amplitudes at the edges of the rightmost and of the leftmost grooves, respectively, and $|H_x^{wg}|$ and $|E_x^{wg}|$ are those at the same positions for the case without grooves, respectively. Fig. 4 shows the calculated dependence of I_r^{TM} and I_r^{TE} with the slit–groove distances d_L and d_R on the left and right sides. It is clear that the slit–groove distances are key parameters as they may lead to enhanced or suppressed launching of the specific polarized mode, and the distances for constructive interference (illustrated by vertical dashed lines) are well predicted by (2).

3. Results and Discussions

In this section, we will analyze and discuss the performance of a BPSA. We should emphasize that this work is intended not to provide an exhausted optimization of geometrical parameters but to present a proof of concept. With the knowledge of Figs. 3 and 4, a detailed analysis will be performed with $p_L = 410$ nm, $w_L = 110$ nm, $h_L = 100$ nm, $d_L = 635$ nm, $p_R = 570$ nm, $w_R = 505$ nm, $h_R = 350$ nm, and $d_R = 1153$ nm.

Fig. 5 illustrates the scattered field distribution $|E_x^{\mathrm{sc}}|$ (a) and (b) under TE-polarized illumination of unitary amplitude of $|E_x^{\mathrm{in}}|$, and $|H_x^{\mathrm{sc}}|$ (c) and (d) under TM-polarized illumination of unitary amplitude

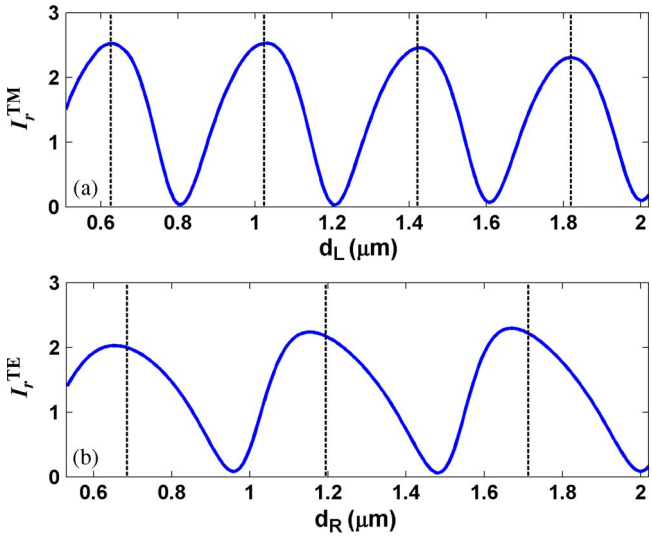

Fig. 4. I_r^{TM} and I_r^{TE} as functions of the slit–groove distances d_L (a) and d_R (b), respectively. The vertical black dashed lines show the distances determined by equation (2) for constructive interference, where $\rho_{N_L}^{TM} = -0.9408 - 0.0055i$, $\tau^{TM} = 0.6555 - 0.3153i$, $\rho_{N_R}^{TE} = -0.6013 - 0.4948i$, and $\tau^{TE} = 0.7073 + 0.2139i$.

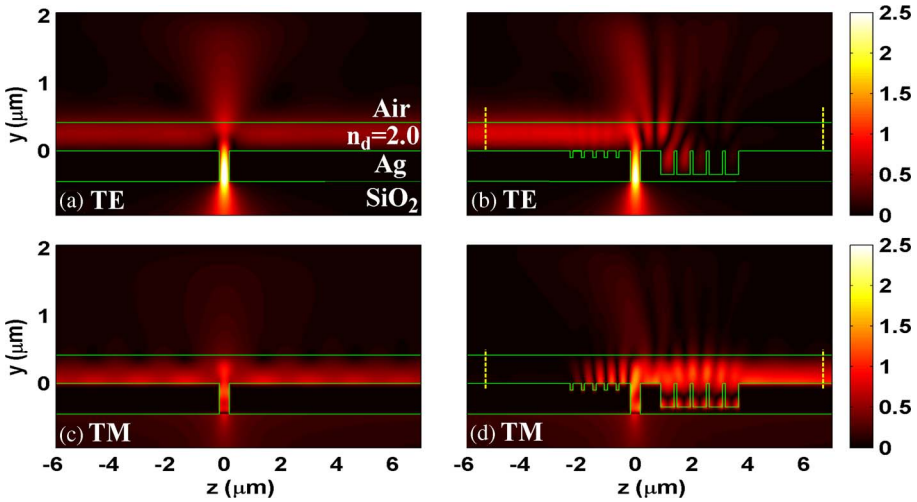

Fig. 5. Scattered field $|E_x^{sc}|$ (a) and (b) under TE-polarized illumination of unitary amplitude of $|E_x^{in}|$, and $|H_x^{sc}|$ (c) and (d) under TM-polarized illumination of unitary amplitude of $|H_x^{in}|$ for the MDA waveguide without (a) and (c) and with (b) and (d) arrays of grooves surrounding the slit, respectively. The calculations are performed with $d_L = 635$ nm and $d_R = 1153$ nm with all other geometrical parameters being the same as those in the previous calculations. The green lines outline structures under analysis. The vertical yellow dashed lines show the positions and intervals of the integrations performed to calculate the energy flow of the TE- and TM-polarized modes.

of $|H_x^{in}|$ for the obtained structure without (a) and (c) and with (b) and (d) arrays of grooves, respectively. It is clear that without grooves, both polarized modes are efficiently excited and launched bidirectionally. Whereas with asymmetric grooves and properly designed slit–groove distances, the left-propagating TE mode and right-propagating TM mode are efficiently launched, and meanwhile, the right-propagating TE mode and left-propagating TM mode are very weak. As expected, the surrounding asymmetric grooves are polarization selective in terms of reflectance and transmittance; the outward radiation scattered by the grooves is small and has little influence on the propagating waveguide modes, as shown in Fig. 5(b) and (d).

To quantitatively evaluate the performance of the proposed structure, we adopt insertion loss (IL), polarization extinction ratio (PER), and crosstalk (CR) as the figures of merit, which are defined as follows:

$$\mathrm{IL}^{\mathrm{TE}} = 10\log\left(P_{\mathrm{in}}^{\mathrm{TE}}/P_{L}^{\mathrm{TE}}\right) \tag{3a}$$

$$\mathrm{IL}^{\mathrm{TM}} = 10\log\left(P_{\mathrm{in}}^{\mathrm{TM}}/P_{R}^{\mathrm{TM}}\right) \tag{3b}$$

$$\mathrm{PER}_{L} = 10\log\left(P_{L}^{\mathrm{TE}}/P_{L}^{\mathrm{TM}}\right) \tag{3c}$$

$$\mathrm{PER}_{R} = 10\log\left(P_{R}^{\mathrm{TM}}/P_{R}^{\mathrm{TE}}\right) \tag{3d}$$

$$\mathrm{CR}^{\mathrm{TE}} = 10\log\left(P_{R}^{\mathrm{TE}}/P_{L}^{\mathrm{TE}}\right) \tag{3e}$$

$$\mathrm{CR}^{\mathrm{TM}} = 10\log\left(P_{L}^{\mathrm{TM}}/P_{R}^{\mathrm{TM}}\right) \tag{3f}$$

where $P_{\mathrm{in}}^{\mathrm{TE;TM}} = \int_{w_s}(\mathbf{E}\times\mathbf{H})\cdot\mathbf{y}dz$ is the energy flow of the incident TE- or TM-polarized plane wave launched onto the slit opening, and $P_{L;R}^{\mathrm{TE;TM}} = \int_{y}(\mathbf{E}\times\mathbf{H})\cdot\mathbf{z}dy$ is that of the TE- or TM-polarized guiding mode at the edge of the leftmost or the rightmost groove. The integration of $P_{L;R}^{\mathrm{TE;TM}}$ along the y-direction is performed between the boundaries of 1/5e decrease of $|E_x^{\mathrm{sc}}|$ for the TE mode or $|H_x^{\mathrm{sc}}|$ for the TM mode (indicated by the vertical yellow dashed lines in Fig. 5), so that most of the energy flow carried by the photonic mode (TE) or the plasmonic mode (TM) is incorporated. Note that $P_{L;R}^{\mathrm{TE;TM}}$ is calculated at a sufficiently far distance of 3 μm away from the edge of the outmost grooves, where the field is dominated by the TE- or TM-polarized mode, then we propagate this energy flow back to the edge of the outmost grooves with the complex effective index of the corresponding mode. In such a way, the possible influences of outward-going radiations are eliminated since our only concern is on the bounded waveguide modes. We emphasize that IL incorporates losses introduced by the scattering at the entrance side of the slit, by the excitation of surface plasmons propagating at the metal/substrate interface (for the TM polarization only), by the out-of-plane scattering (leakage) at the exit side of the slit and at grooves, and by the intrinsic absorption of the metal. This is better understood with the definition of coupling efficiency: $\eta^{\mathrm{TE}} = P_{L}^{\mathrm{TE}}/P_{\mathrm{in}}^{\mathrm{TE}}$ for the TE polarization or $\eta^{\mathrm{TM}} = P_{R}^{\mathrm{TM}}/P_{\mathrm{in}}^{\mathrm{TM}}$ for the TM polarization. PER is concerned about the energy flow of different polarizations in the same direction, whereas CR is defined in terms of the energy flow of identical polarization in different directions.

For the case of incident wavelength $\lambda = 1550$ nm, as shown in Fig. 5, exciting performance is obtained: $\mathrm{IL}^{\mathrm{TE}} = 2.39$ dB $(\eta^{\mathrm{TE}} = 57\%)$ and $\mathrm{IL}^{\mathrm{TM}} = 3.25$ dB $(\eta^{\mathrm{TM}} = 47\%)$, $\mathrm{PER}_{L} = 27.04$ dB and $\mathrm{PER}_{R} = 24.74$ dB, and $\mathrm{CR}^{\mathrm{TE}} = -25.60$ dB and $\mathrm{CR}^{\mathrm{TM}} = -26.18$ dB. The small difference between $\mathrm{IL}^{\mathrm{TE}}$ and $\mathrm{IL}^{\mathrm{TM}}$ is beneficial for the practical applications. These results are of great importance from both a theoretical point of view and for its use in highly integrated polarization-transparent diversity systems and optical signal processing in photonic integrated circuit.

The spectral performances of these figures of merit are illustrated in Fig. 6(a)–(c). As shown in Fig. 6(a), the ILs less than 4 dB, i.e., more than 40 % coupling efficiency, are achieved for both polarizations in the wavelength range 1510–1570 nm. In this wavelength range, the PERs better than 18 dB and CR less than -18 dB are achieved for both polarizations. The proposed structure can also function as an efficient unidirectional launcher for TE- or TM-polarized light or as an integrated polarization analyzer. For such functionalities, the efficiency coefficient E_r defined as the quotient between the coupling efficiency of the right (or left)-propagating TM (or TE) mode with grooves on both sides and without any grooves could be used to characterize the performance, as was done in [6] and [22]. The spectral performance of E_r is shown in Fig. 6(d). It is clear that E_r is close to or larger than 2.0 for both polarizations in the wavelength range 1510–1570 nm. Note that E_r may be close to I_r in values as they are both used to evaluate the directional enhancement. We should emphasize that the polarization-selective asymmetric grooves and properly designed slit–groove distances enhance the propagation of TM- and TE-polarized modes, enabling two polarizations to be unidirectionally launched, respectively.

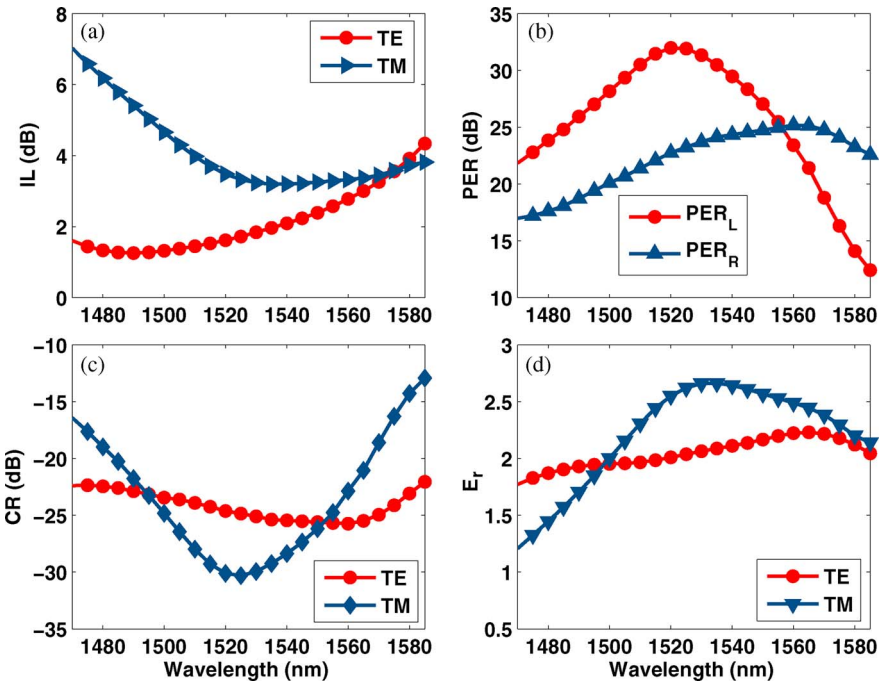

Fig. 6. The spectral (a) IL, (b) PER, (c) CR, and (d) E_r for TE- and TM-polarized modes.

4. Conclusion

In conclusion, we have proposed and theoretically investigated a compact BPSA composed of the asymmetric polarization-selective grooves surrounding a nanoslit in the MDA configuration. A theory on the analysis of the groove array and slit–groove distances has been developed and validated by the fully vectorial a-FMM calculations. With the properly designed asymmetric grooves and slit–groove distances, the TM- and TE-polarized modes supported by the MDA waveguide are split and launched into opposite propagating directions, which elucidates the design concept of the structure. Numerical simulations show that ILs less than 4 dB, PERs better than 18 dB, and CR less than −18 dB for both polarizations are achieved in the wavelength range 1510–1570 nm. The structure could also serve as an efficient unidirectional polarizer or an integrated polarization analyzer, and will be promising for the utilization of both polarizations in plasmonic circuitry. We believe that the proposed BPSA could be of great interest for potential applications in polarization-transparent microphotonic devices, nanoscale photonic circuitry, and optical interconnects and polarization analysis on chips.

References

[1] T. Barwicz, M. R. Watts, M. A. Popović, P. T. Rakich, L. Socci, F. X. Kärtner, E. P. Ippen, and H. I. Smith, "Polarization-transparent microphotonic devices in the strong confinement limit," *Nat. Photon.*, vol. 1, no. 1, pp. 57–60, Jan. 2007.
[2] H. Fukuda, K. Yamada, T. Tsuchizawa, T. Watanabe, H. Shinojima, and S. Itabashi, "Silicon photonic circuit with polarization diversity," *Opt. Exp.*, vol. 16, no. 7, pp. 4872–4880, Mar. 2008.
[3] V. Gruev, J. Van de Spiegel, and N. Engheta, "Dual-tier thin film polymer polarization imaging sensor," *Opt. Exp.*, vol. 18, no. 18, pp. 19 292–19 303, Aug. 2010.
[4] R. Zia, J. A. Schuller, A. Chandran, and M. L. Brongersma, "Plasmonics: The next chip-scale technology," *Mater. Today*, vol. 9, no. 7/8, pp. 20–27, Jul.-Aug. 2006.
[5] S. A. Maier, *Plasmonics: Fundamentals and Applications*. New York: Springer-Verlag, 2007.
[6] F. López-Tejeira, S. G. Rodrigo, L. Martín-Moreno, F. J. García-Vidal, E. Devaux, T. W. Ebbesen, J. R. Krenn, I. P. Radko, S. I. Bozhevolnyi, M. U. González, J. C. Weeber, and A. Dereux, "Efficient unidirectional nanoslit couplers for surface plasmons," *Nat. Phys.*, vol. 3, no. 5, pp. 324–328, May 2007.
[7] P. Chen, Q. Gan, F. J. Bartoli, and L. Zhu, "Near-field-resonance-enhanced plasmonic light beaming," *IEEE Photon. J.*, vol. 2, no. 1, pp. 8–17, Feb. 2010.

[8] Q. Gan and F. J. Bartoli, "Bidirectional surface wave splitter at visible frequencies," *Opt. Lett.*, vol. 35, no. 24, pp. 4181–4183, Dec. 2010.
[9] A. Baron, E. Devaux, J.-C. Rodier, J.-P. Hugonin, E. Rousseau, C. Genet, T. W. Ebbesen, and P. Lalanne, "Compact antenna for efficient and unidirectional launching and decoupling of surface plasmons," *Nano Lett.*, vol. 11, no. 10, pp. 4207–4212, Oct. 2011.
[10] J. S. Q. Liu, R. A. Pala, F. Afshinmanesh, W. Cai, and M. L. Brongersma, "A submicron plasmonic dichroic splitter," *Nat. Commun.*, vol. 2, p. 525, Nov. 2011.
[11] B. Wang and G. P. Wang, "Directional beaming of light from a nanoslit surrounded by metallic heterostructures," *Appl. Phys. Lett.*, vol. 88, no. 1, pp. 013114-1–013114-3, Jan. 2006.
[12] Z. Fu, Q. Gan, K. Gao, Z. Pan, and F. J. Bartoli, "Numerical investigation of a bidirectional wave coupler based on plasmonic Bragg gratings in the near infrared domain," *J. Lightw. Technol.*, vol. 26, no. 22, pp. 3699–3703, Nov. 2008.
[13] L. Chen, G. P. Wang, Q. Gan, and F. J. Bartoli, "Trapping of surface-plasmon polaritons in a graded Bragg structure: Frequency-dependent spatially separated localization of the visible spectrum modes," *Phys. Rev. B, Condens. Matter*, vol. 80, no. 16, pp. 161106-1–161106-4, Oct. 2009.
[14] S. I. Bozhevolnyi, Ed., *Plasmonic Nanoguides and Circuits*. Singapore: Pan Stanford Publ., 2008.
[15] A. Seidel, C. Reinhardt, T. Holmgaard, W. Cheng, T. Rosenzveig, K. Leosson, S. I. Bozhevolnyi, and B. N. Chichkov, "Demonstration of laser-fabricated DLSPPW at telecom wavelength," *IEEE Photon. J.*, vol. 2, no. 4, pp. 652–658, Aug. 2010.
[16] D. Kalavrouziotis, S. Papaioannou, G. Giannoulis, D. Apostolopoulos, K. Hassan, L. Markey, J.-C. Weeber, A. Dereux, A. Kumar, S. I. Bozhevolnyi, M. Baus, M. Karl, T. Tekin, O. Tsilipakos, A. Pitilakis, E. E. Kriezis, H. Avramopoulos, K. Vyrsokinos, and N. Pleros, "0.48 Tb/s (12 $\times$ 40 Gb/s) WDM transmission and high-quality thermo-optic switching in dielectric loaded plasmonics," *Opt. Exp.*, vol. 20, no. 7, pp. 7655–7662, Mar. 2012.
[17] W. Bogaerts, D. Taillaert, P. Dumon, D. Van Thourhout, and R. Baets, "A polarization-diversity wavelength duplexer circuit in silicon-on-insulator photonic wires," *Opt. Exp.*, vol. 15, no. 4, pp. 1567–1578, Feb. 2007.
[18] C. R. Doerr, P. J. Winzer, Y.-K. Chen, S. Chandrasekhar, M. S. Rasras, L. Chen, T.-Y. Liow, K.-W. Ang, and G.-Q. Lo, "Monolithic polarization and phase diversity coherent receiver in silicon," *J. Lightw. Technol.*, vol. 28, no. 4, pp. 520–525, Feb. 2010.
[19] E. Moreno, L. Martín-Moreno, and F. J. García-Vidal, "Extraordinary optical transmission without plasmons: The s-polarization case," *J. Opt. A, Pure Appl. Opt.*, vol. 8, no. 4, pp. S94–S97, Mar. 2006.
[20] M. Guillaumée, A. Y. Nikitin, M. J. K. Klein, L. A. Dunbar, V. Spassov, R. Eckert, L. Martín-Moreno, F. J. García-Vidal, and R. P. Stanley, "Observation of enhanced transmission for s-polarized light through a subwavelength slit," *Opt. Exp.*, vol. 18, no. 9, pp. 9722–9727, Apr. 2010.
[21] A. Y. Nikitin, F. J. García-Vidal, and L. Martín-Moreno, "Enhanced optical transmission, beaming and focusing through a subwavelength slit under excitation of dielectric waveguide modes," *J. Opt. A, Pure Appl. Opt.*, vol. 11, no. 12, pp. 125 702-1–125 702-8, Sep. 2009.
[22] A. Y. Nikitin, F. J. García-Vidal, and L. Martín-Moreno, "Intercoupling of free-space radiation to s-polarized confined modes via nanocavities," *Appl. Phys. Lett.*, vol. 94, no. 6, pp. 063119-1–063119-3, Feb. 2009.
[23] T. Holmgaard and S. I. Bozhevolnyi, "Theoretical analysis of dielectric-loaded surface plasmon-polariton waveguides," *Phys. Rev. B*, vol. 75, no. 24, pp. 245405-1–245405-12, Jun. 2007.
[24] L. Yin, V. K. Vlasko-Vlasov, A. Rydh, J. Pearson, U. Welp, S.-H. Chang, S. K. Gray, G. C. Schatz, D. B. Brown, and C. W. Kimball, "Surface plasmons at single nanoholes in Au films," *Appl. Phys. Lett.*, vol. 85, no. 3, pp. 467–469, Jul. 2004.
[25] E. Popov, N. Bonod, M. Neviére, H. Rigneault, P.-F. Lenne, and P. Chaumet, "Surface plasmon excitation on a single subwavelength hole in a metallic sheet," *Appl. Opt.*, vol. 44, no. 12, pp. 2332–2337, Apr. 2005.
[26] E. D. Palik, *Handbook of Optical Constants of Solids*. New York: Academic, 1985.
[27] K. Uchida, "Numerical analysis of surface-wave scattering by finite periodic notches in a ground plane," *IEEE Trans. Microw. Theory Tech.*, vol. MTT-35, no. 5, pp. 481–486, May 1987.
[28] G. Li, L. Cai, F. Xiao, Y. Pei, and A. Xu, "A quantitative theory and the generalized Bragg condition for surface plasmon Bragg reflectors," *Opt. Exp.*, vol. 18, no. 10, pp. 10 487–10 499, May 2010.
[29] G. Li, F. Xiao, L. Cai, K. Alameh, and A. Xu, "Theory of the scattering of light and surface plasmon polaritons by finite-size subwavelength metallic defects via field decomposition," *New. J. Phys.*, vol. 13, no. 7, p. 073045, Jul. 2011.
[30] E. Silberstein, P. Lalanne, J.-P. Hugonin, and Q. Cao, "Use of grating theories in integrated optics," *J. Opt. Soc. Amer. A, Opt. Image Sci.*, vol. 18, no. 11, pp. 2865–2875, Nov. 2001.